

# A novel dynamic integral sliding mode control for power electronic converters

Science Progress

2021, Vol. 104(4) 1–16

© The Author(s) 2021

Article reuse guidelines:

sagepub.com/journals-permissions

DOI: 10.1177/00368504211044848

journals.sagepub.com/home/sci



Mudassar Riaz<sup>1</sup> , Abdul Rehman Yasin<sup>1</sup> , Ali Arshad Uppal<sup>2</sup> and Amina Yasin<sup>3</sup>

<sup>1</sup>Department of Electrical Engineering, The University of Lahore, Pakistan

<sup>2</sup>Department of Electrical and Computer Engineering, COMSATS University Islamabad, Islamabad, Pakistan

<sup>3</sup>Department of Basic Sciences, Preparatory Year Deanship, King Faisal University, Saudi Arabia

## Abstract

The key characteristics of the sliding mode control (SMC) are the ability to manage unmodeled dynamics with rapid response and the inherent robustness of parametric differences, making it an appropriate choice for the control of power electronic converters. However, its drawback of changing switching frequency causes critical electro-magnetic compatibility and switching power loss issues. This paper addresses the problem by proposing a dynamic integral sliding mode control for power converters having fixed switching frequency. A special hardware test rig is developed and tested under unregulated 12.5–22.5 V input and 30 V output. The experimental findings indicate excellent controller efficiency under wide range of loads and uncertain input voltage conditions. In addition, the findings indicate that the closed-loop system is robust to sudden differences in load conditions. This technique provides an improvement of 24.52% in the rise time, 20.10% in the settling time and 42.85% in robustness of the controller as compared to conventional controllers. Furthermore, the comparison with the existing fixed-frequency sliding mode control techniques is presented in a tabular form.

## Keywords

Power converter, non-linear controllers, fixed frequency, sliding mode control (SMC)

## Introduction

Advanced applications such as integration of renewable energy resources with microgrids require robustness and precise voltage control.<sup>1–5</sup> In the existence of parametric and

### Corresponding author:

Mudassar Riaz, Department of Electrical Engineering, The University of Lahore, Lahore, Pakistan.

Email: mudassarriaz041@gmail.com



Creative Commons Non Commercial CC BY-NC: This article is distributed under the terms of the Creative Commons Attribution-NonCommercial 4.0 License (<https://creativecommons.org/licenses/by-nc/4.0/>)

which permits non-commercial use, reproduction and distribution of the work without further permission provided the original work is attributed as specified on the SAGE and Open Access page (<https://us.sagepub.com/en-us/nam/open-access-at-sage>).

internal uncertainties, conventional non-linear control techniques do not provide required robustness.<sup>6–8</sup> Therefore, the sliding mode control (SMC) becomes a good candidate for controlling such systems with unknown dynamics and uncertain parameters with external perturbations.<sup>9,10</sup> In addition, SMC provides better transient response due to its ability to utilize all the available system gains.

A discontinuous function is the natural way to implement a SMC, but its use is limited by the ideal requirement of infinite switching frequency. A realistic approach has been reported in Sabanovic et al.<sup>11</sup> and Venkataramanan<sup>12</sup> where a hysteresis comparator substitutes the discontinuous *sign* function, thus forcing the switch to operate at a finite frequency. Although a finite frequency of switching is achieved, it is variable and dependent on the system states.<sup>13</sup> The finite switching frequency causes the output to chatter between bounds which is acceptable for realistic systems. However, the variable switching frequency is not acceptable for power converters because it causes electro-magnetic compatibility (EMC) issues along with complicating the design for its suppression.<sup>14–16</sup>

Hence, fixing the switching frequency in SMC is an active research topic in the field of power electronic converters.<sup>17,18</sup> Interesting results are reported for phase shifted full-bridge converters,<sup>19</sup> interleaved buck converters<sup>16</sup>, current control of permanent-magnet synchronous machines,<sup>20</sup> cascaded boost converters<sup>21</sup> and AC–DC converters.<sup>22</sup> It is important to mention that SMC in power converters needs to operate at constant frequency as they are made up of reactive components whose correct sizing heavily depends upon the switching rate. A solution to this problem is proposed by the authors in Repecho et al.<sup>23</sup> where a technique for fixing the frequency for hysteresis band SMC is reported.

An adaptive controller for the hysteresis band is proposed in, Qi et al.<sup>15</sup>, Repecho et al.<sup>16</sup>, Yasin et al.<sup>18</sup> and Ortiz-Castrillón et al.<sup>24</sup> where the hysteresis width is adjusted such that the resulting switching frequency remains constant. However, the technique requires optimal knowledge of the plant parameters in order to properly adjust its width. The use of additional sensors for parameter sensing increase the cost and limit its applications. Researchers in Repecho et al.<sup>16</sup> have proposed a fixed-frequency SMC by utilizing an external signal. The involvement of new hardware and the requirement of this technique to work under the constraints that the reciprocal of the switching frequency shall be low enough as compared to the system time constant, are its drawbacks.

To achieve a fixed switching frequency, the technique zero average dynamics (ZAD) is used.<sup>25,26</sup> In ZAD, the main objective is to calculate a duty cycle such that the average dynamics of the chosen sliding manifold equals zero. As a result, the steady-state switching time is set to a desired value and the overall average performance is close to the ideal sliding mode. The main drawbacks of ZAD are its complex calculations and requirements of real-time fast processing units.

A method based upon the direct implementation of an ideal equivalent control calculated from the first derivative of the desired switching manifold has been reported by the authors of Yasin et al.<sup>10,27</sup>, Li et al.<sup>28</sup> and Tan et al.<sup>29</sup> However, this approach does not directly implement a discontinuous function which may result in reduced robustness and loss of order reduction. Fixed-switching frequency SMC designs are also achieved through pulse-width modulation (PWM) implementation were introduced in Abrishamifar et al.<sup>30</sup> and Ye et al.<sup>31</sup> In this method, the control law is straightened into a limiting layer to reduce the chattering effects at the cost of reduced robustness of SMC.

The constant switching frequency in SMC has been reported in Huerta et al.<sup>32</sup>, Vidal-Idiarte et al.<sup>33</sup> and Yan et al.<sup>34</sup> using an extra proportional–integral (PI) control loop that controls the width of the hysteresis. In this technique, the designer should ensure that the dynamics of this additional PI loop must be slow enough in order to avoid interference with current and voltage control loops. Drawbacks of this scheme are the additional control loop and the complex calculations.

In this research a novel dynamic integral sliding mode controller is proposed for power electronic converters, which is capable to counter parameter uncertainties and external disturbances. An integral sliding manifold is proposed such that the reaching phase of SMC is eliminated and the effect of both matched and unmatched uncertainties is significantly reduced thereby increasing the robustness of the system. The control signal provided by this technique is continuous in nature and PWM of this signal yields a fixed frequency sequence for the electronic switch. Moreover, this manuscript sheds light on various other fixed-frequency SMC techniques, briefly comparing their methodology and categorization. The comparison of the techniques is based upon their number of sensors, robustness, cost, conversion speed and implementation complexity.

The rest of the paper has the following arrangements: The description of the system and its mathematical model is explained in the section ‘System description and modelling’ and the controller design is presented in the section ‘Dynamic integral sliding mode controller design’. The experimental findings are discussed in the section ‘Hardware results’. The comparison of different fixed-frequency SMC techniques is discussed in the section ‘Comparison of fixed-frequency SMC techniques’ while the article is concluded in the section ‘Conclusion’.

## System description and modelling

Figure 1 shows a conventional boost converter circuit framework in which  $V_{in}$  indicates the input voltage,  $V_{out}$  is the output voltage,  $R$  is the load resistance,  $C$  is the output filter capacitance and  $L$  is the coil inductance. By the application of basic circuit analysis laws, the non-linear dynamics of the system is define as follows:

$$\begin{aligned} \dot{I}_L &= \frac{(u-1)}{L} V_{out} + \frac{1}{L} V_{in}, \\ \dot{V}_{out} &= \frac{(1-u)}{C} I_L + \frac{1}{(R_0 - \Delta R)C} V_{out}. \end{aligned} \quad (1)$$

where  $R = R_0 - \Delta R$  is the actual load resistance,  $\Delta R$  represents the uncertainty in  $R$  and  $R_0$  is the nominal value of the resistance.

In order to simplify mathematical analysis, replace  $\tilde{u} = (1 - u)$ , where  $u$  is the signal input which is used to operate power electronics converters in ON and OFF states, the control signal can be defined as follows:

$$u = \begin{cases} 0 & \text{Switch is in off state} \\ 1 & \text{Switch is in on state} \end{cases}.$$

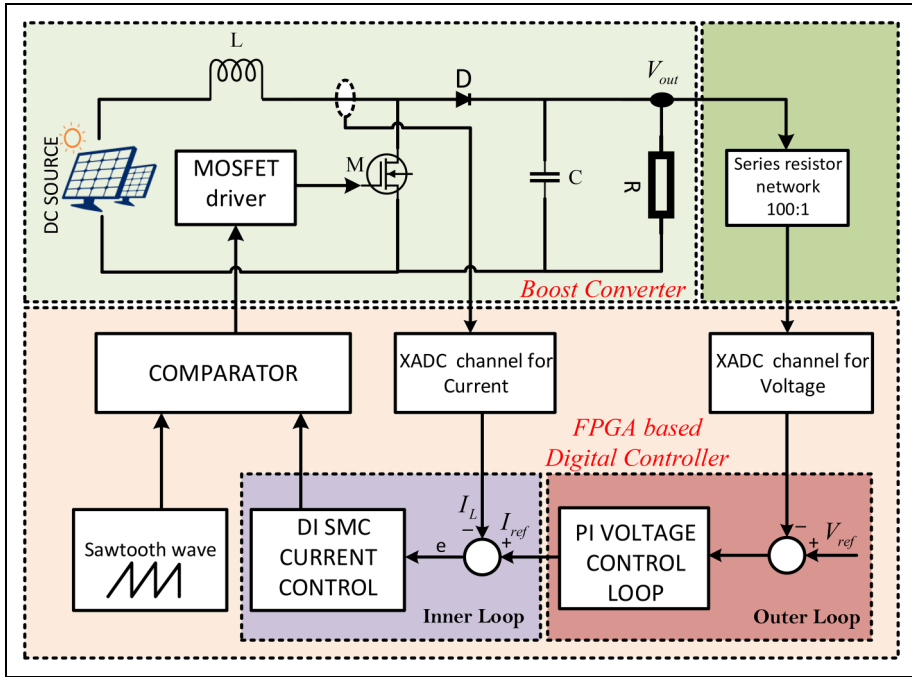


**Figure 1.** Block diagram of the proposed technique.

The DC–DC boost converters are non-linear and non-minimum phase in nature, which making it more difficult to regulate as compared to other power converters. The system becomes unstable if the output voltage is the only variable to be controlled. However, the issue is resolved by a cascade system, where the inductor current and output voltage are controlled by a two-loop structure. The internal loop controls the current of the inductor while the external loop controls the voltage of the load. The internal control loop is modelled using fixed-frequency SMC while the PI controller designs the outer control loop with slower dynamics.

## Dynamic integral sliding mode controller design

In this section, the design procedure for the dynamic integral sliding mode controller (DISMC) for the boost converter is discussed. This hybrid controller combines the properties of both dynamic and integral SMC algorithms. It provides a smooth control signal along with the advantage of eliminating the reaching phase, which increases the robustness of the closed-loop system. The output of the controller is a continuous signal which is pulse width modulated to achieve fixed-frequency DISMC. The control input to achieve the required performance and robustness has two parts

$$\dot{\hat{u}} = \dot{\hat{u}}_0 + \dot{\hat{u}}_1. \quad (2)$$

### Design of continuous part

The continuous part  $\dot{\tilde{u}}_0$  is designed using pole placement technique, whereas the discontinuous part of the controller  $\dot{\tilde{u}}_1$  ensures the existence of sliding mode in the presence of external disturbances. The continuous part is given as

$$\tilde{u}_0 = -\eta e - k \int e dt, \quad (3)$$

where  $e = I_{ref} - I_L$  while  $\eta, : k \in \mathfrak{R}^+$  are controller gains. The integral type sliding surface that achieves the desired performance and robustness is characterized as

$$S = \sigma(e) + z(t), \quad (4)$$

$$\sigma(e) = \dot{e} + \lambda e, \quad (5)$$

where  $z(t)$  is the integral term and is defined as

$$\dot{z} = \lambda \dot{e} - \dot{\tilde{u}}_0 \quad \text{with} \quad z(0) = -\sigma(e). \quad (6)$$

Taking time derivative of (4) and using (5) and (6) we get

$$\dot{S} = \ddot{e} - \dot{\tilde{u}}_0. \quad (7)$$

by taking the derivative,  $e$  will become

$$\begin{aligned} \dot{e} &= \dot{I}_{ref} - \dot{I}_L \\ \dot{e} &= \dot{I}_{ref} + \frac{\tilde{u}}{L} V_{out} - \frac{1}{L} V_{in} \end{aligned} \quad (8)$$

### Design of discontinuous part

Taking the first derivative of (8) we get

$$\ddot{e} = \ddot{I}_{ref} + \frac{\dot{\tilde{u}}}{L} V_{out} - \frac{1}{L} \dot{V}_{in} + \frac{\tilde{u}^2}{LC} I_L + \frac{\tilde{u}}{R_0 LC} V_{out} \quad (9)$$

Substituting the value of  $e$  and involving the dynamics of system from (1) we get

$$\begin{aligned} \dot{S} &= \ddot{I}_{ref} + \frac{1}{L} \dot{\tilde{u}} V_{out} - \frac{1}{L} \dot{V}_{in} \\ &+ \frac{1}{LC} \tilde{u}^2 I_L + \frac{1}{R_0 LC} \tilde{u} V_{out} - \dot{\tilde{u}}_0 \end{aligned} \quad (10)$$

In order to ensure the existence of sliding mode, following reachability condition shall be satisfied:

$$\dot{S} = -M \text{sign}(S); \quad M \in \mathfrak{R}^+. \quad (11)$$

By using (10) and (11), we design the discontinuous controller as

$$\begin{aligned} -Msign(S) &= (\dot{\tilde{u}}_0 + \dot{\tilde{u}}_1) \frac{1}{L} V_{out} + \ddot{I}_{ref} \\ &\quad - \frac{1}{L} \dot{V}_{in} + \frac{1}{LC} \tilde{u}^2 I_L + \frac{1}{R_0 LC} \tilde{u} V_{out} - \dot{\tilde{u}}_0 \end{aligned} \quad (12)$$

$$\begin{aligned} \dot{\tilde{u}}_1 &= -\frac{L}{V_{out}} \left[ Msign(S) + \ddot{I}_{ref} - \frac{1}{L} \dot{V}_{in} - \dot{\tilde{u}}_0 \right. \\ &\quad \left. \left( 1 - \frac{V_{out}}{L} \right) + \frac{1}{LC} \tilde{u}^2 I_L + \frac{1}{R_0 LC} V_{out} \tilde{u} \right] \end{aligned} \quad (13)$$

The discontinuous control in (13) is practically realizable as both the states  $V_{out}$  and  $I_L$  are measurable. The dynamic control input is obtained by substituting  $\dot{\tilde{u}}_1$ , equation (13) and  $\dot{\tilde{u}}_0$ , equation (3) in (2). Consequently, a continuous control signal is obtained by integrating (2), which is pulse width modulated to achieve the desired switching frequency.

### Existence of the sliding mode

The existence of the sliding mode can be proved by considering the following Lyapunov functional:

$$V(x, t) = \frac{1}{2} S^2. \quad (14)$$

The time derivative of (14) takes the form

$$\dot{V}(x, t) = S\dot{S}. \quad (15)$$

Substituting the value of  $\dot{S}$  in (15) we get

$$\begin{aligned} \dot{V}(x, t) &= S \left[ \ddot{I}_{ref} + \frac{1}{L} \dot{\tilde{u}}_1 V_{out} + \frac{1}{L} \dot{\tilde{u}}_0 V_{out} - \frac{1}{L} \dot{V}_{in} \right. \\ &\quad \left. + \frac{1}{LC} \tilde{u}^2 I_L + \frac{1}{(R_0 - \Delta R)LC} \tilde{u} V_{out} - \dot{\tilde{u}}_0 \right]. \end{aligned} \quad (16)$$

By substituting  $\dot{\tilde{u}}_1$ , cf. equation (13) in the above equation yields

$$\dot{V}(x, t) = -S \left[ Msign(S) - \frac{\Delta R V_{out} \tilde{u}}{R_0 (R_0 - \Delta R) LC} \right],$$

where  $\Delta R \leq \Pi$  and  $\Pi$  is the maximum value of uncertainty in the load resistance.

Using the upper bound on  $\Delta R$  the time derivative of the Lyapunov functional becomes

$$\dot{V}(x, t) \leq -|S| \left[ M - \frac{\Pi V_{out} \tilde{u}}{R_0(R_0 - \Pi)LC} \right]. \quad (17)$$

Now if  $M$  is chosen such that  $M > \frac{\Pi V_{out} \tilde{u}}{R_0(R_0 - \Pi)LC} + \varphi$ , where  $\varphi \in \mathfrak{R}^+$  &  $\Pi = 72$  then the time derivative of the lyapunov functional is negative definite. Hence, the sliding mode occurs in the manifold  $S = 0$  in finite time.

## Hardware results

The results presented here are based on a boost converter parameters presented in Table 1 having filter capacitance of  $C = 2000 \mu\text{F}$  and a coil inductance  $L = 100 \mu\text{H}$ . The switch consists of, *IRF540* N-channel metal oxide field effect transistor (MOSFET) having low Drain to Source on resistance ( $< 20 \text{ m}\Omega$ ) and medium current handling capabilities (20–28 A).

The switching sequence is provided by the FPGA-based system that controls the current of the inductor. The system is operated at 32 kHz switching frequency. The output voltages are first transformed to lower voltages (100:1) by a series resistive network since the nominal voltages for analogue to digital converter (ADC) channel of FPGA (CPG 236) is 1 V. A voltage buffer is used to feed these reduce voltages to the ADC channel. Inductor current is fed to FPGA in the similar manner except that the conversion ratio used is (1:1). After taking 10 samples the average is calculated for the error computations. Each average is computed at the end of  $20 \mu\text{s}$  taking a sample after every  $2 \mu\text{s}$ . It is important to mention that careful calculations must be carried out while handling the fractional part of real numbers and signed variables in Verilog, a hardware descriptive language (HDL). Whereas, in C language this is handled by default. It is important to note that higher switching frequencies reduce component sizes but increase switching losses. The selection of the switching frequency, therefore, constitutes a compromise between efficiency and power quality. The inductor current is measured by placing a  $0.47 \Omega$  resistance in its return path and then providing a gain of 2.1 via an operational amplifier. The experimental results are obtained using RIGOL oscilloscope with two 70 MHz bandwidth channels. The maximum rate of sampling is 1 G samples/s. The experimental setup is shown in Figure 2. The input voltage of the converter is switched to 400 MHz to get the step response

**Table 1.** Boost converter parameters.

Specification	Representation	Value
Input voltage	$V_{in}$	12 V
Output voltage	$V_{out}$	30 V
Capacitance	$C$	2000 $\mu\text{F}$
Coil inductance	$L$	100 $\mu\text{H}$
Switching frequency	$S_f$	32 kHz
Load resistor	$R_0$	60 $\Omega$
Variation in load	$\Delta R$	0–40 $\Omega$

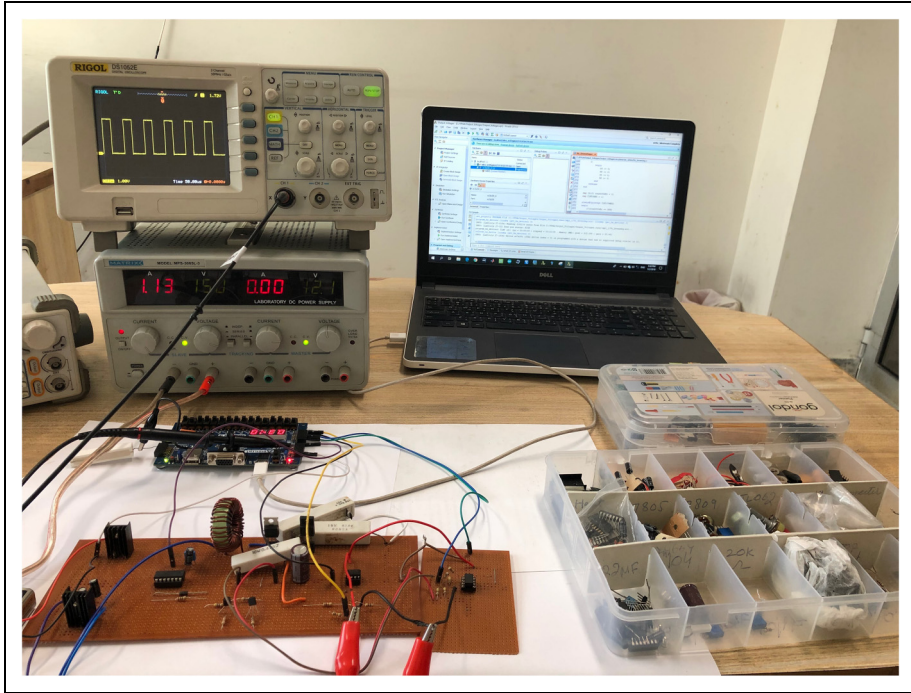


**Figure 2.** Experimental setup to evaluate the performance of the controllers.

of the system. A PNP power transistor, TIP147, connects and disconnects  $V_{in}$  according to a 400 MHz square wave to perform the switching action.

### *Step response and steady-state error*

The performance of the controller is tested under different load conditions. The input voltage of the converter is switched to 400 MHz to get the step response of the system. A PNP power transistor, TIP147, connects and disconnects  $V_{in}$  according to a 400 MHz square wave to perform the switching action. The complete response of closed-loop system is shown in Figure 3. For different load conditions ( $20\ \Omega \leq R_L \leq 100\ \Omega$ ), the controller maintains 30 V at the output with zero steady-state error. As illustrated in Figure 3(a), the suggested controller has a rise time of 26.33 ms and a settling time of 50.32 ms for a simulated result. The experimental rise time and setting time of the purposed controller are 31.60 and 56.02 ms, respectively, as shown in Figure 3(b). The disparity between simulated and experimental outcomes is due to the fact that experimental results are based on a real-time system rather than a simulation. A simulation of the inductor current step response is presented in Figure 3(c), whereas an experimental step response is provided in Figure 3(d). In its most basic form, a boost converter is based on an inductor's ability to withstand changes in current by increasing or decreasing the amount of energy stored within the inductor magnetic field. The change in inductor



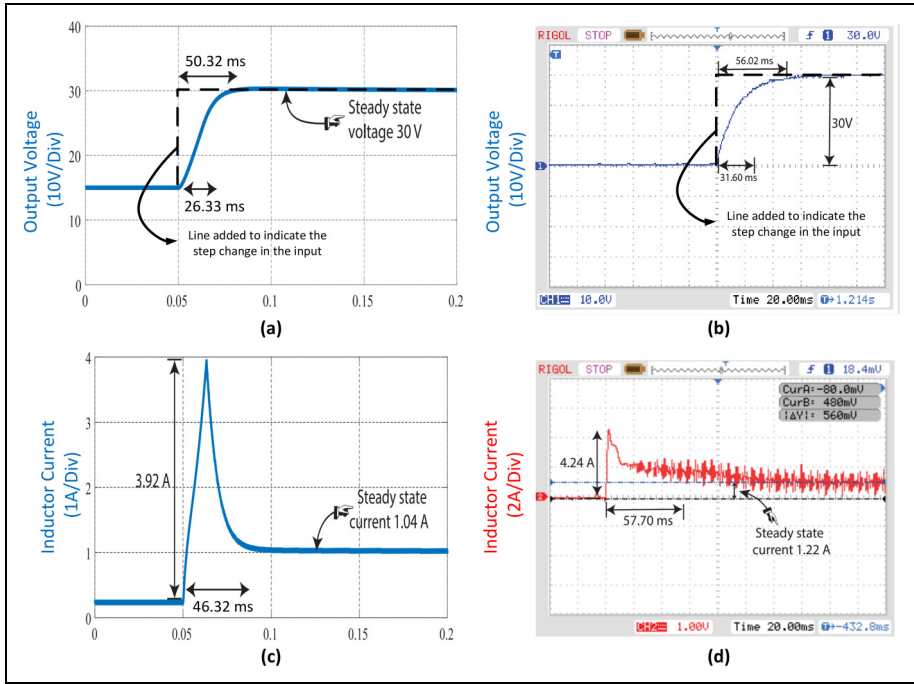


**Figure 3.** Dynamic integral sliding mode controller (DISMC) simulations and experiments for the closed loop system are presented. (a) Simulated step response of the system. (b) Experimental step response of the system. (c) Simulated inductor current during start up. (d) Experimental inductor current during start up.

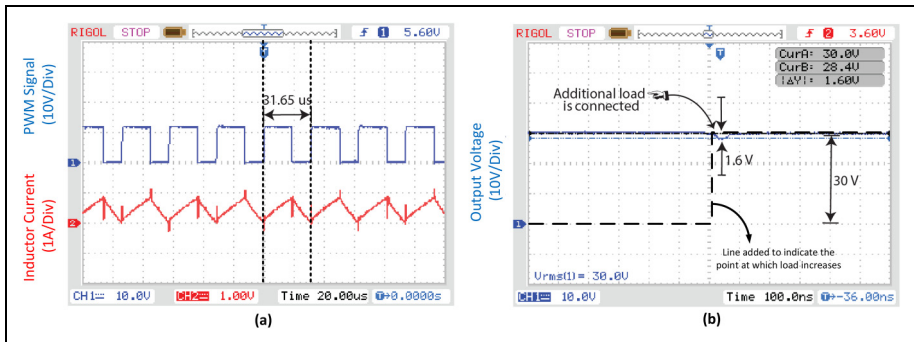


**Figure 4.** Experimental results for close-loop system with Dynamic integral sliding mode controller (DISMC). (a) Gating signal with inductor current. (b) Response of the system when additional load is connected.

current with a fixed PWM signal provided by the controller can be monitored in Figure 4(a) to verify that the controller is providing the correct signal.

**Robustness**

In order to verify the robustness of the controller, and to note its behavior under changing load conditions, a setup is designed to change the load resistance from 100 to 31.97  $\Omega$ . This is achieved by switching a 100  $\Omega$  parallel resistor to the existing 47  $\Omega$  parallel load. A power transistor TIP147 (PNP) operated by C1383 (NPN) used for switching extra load at 10 kHz frequency. The system recovers the change in the step load in less than 85 ns, as shown in Figure 4(b). This shows the disturbance rejection of the proposed technique, which is an inherent property of SMC. In addition, the controller’s performance is also tested under variable input voltages 12.5–22.5 V and it is observed the output voltage remains constant 30 V. The controller works efficiently and the results are summarized in Table 2.

**Comparison of fixed-frequency SMC techniques**

With the number of techniques to fix the frequency in SMC, it may not be trivial for a researcher to choose between these techniques. Therefore, to help the reader a comparison between the proposed and the existing techniques is presented in this section based upon the following highlighted aspects.

**Implementation**

The simplicity to implement a certain technique is a key factor in deciding which fixed frequency technique shall be used for a particular application. However, the ease of implementation directly depends upon the knowledge of the users and their relative experience. In literature both analogue (using operational amplifiers) and digital (involving micro-controllers and microprocessors) techniques are encountered for the implementation of fixed-frequency SMC techniques.

**Sensors**

The number and type of sensors required for a particular technique is also an important factor that effects the selection process. Generally, it is easy and cost effective to

**Table 2.** Output voltages for input variation.

Input voltage $V_{in}$	Output voltage $V_{out}$
12.5	30 V
15.0	30 V
17.5	30 V
20.0	30 V
22.5	30 V

measure voltage as compared to current, because for large current applications ( $>10\text{ A}$ ), the sensors become bulky and expensive. It shall be noted that due to the non-minimum phase nature of boost converters, the voltage regulation problem has to be addressed in terms of cascade control. Therefore, it requires both voltage and current sensors to solve the problem in contrast with buck converter that can be controlled using voltage sensors only.

Cost

The cost of each technique cannot be specified unless it is physically implemented. However, a comparison can be made on the basis of analogue or digital circuitry, requirement of software programing or hardware setup and the number of sensors used. Generally, analogue circuits are cheaper when compared with digital circuits having programmable chips.

Dynamic response

Dynamic response including rise and settling times are an important parameter to evaluate the controller performance. However, unfortunately these parameters cannot be discussed in tabular form as exact details could not be found unless and until these techniques are implemented on a system having same parameters. For the comparison a conventional PI was designed and tested on a same parameters of the system. In comparison with PI controller as shown in Figure 5 this technique provides an improvement of 24.52% in the rise time and 20.10% in the settling time as compared to conventional PI controllers. Moreover an improvement of 42.85% is also observed in the robustness of the controller.

Applications

It is extremely important to consider the application in which a technique will be employed before selecting a technique. For example, in the case of voltage control in

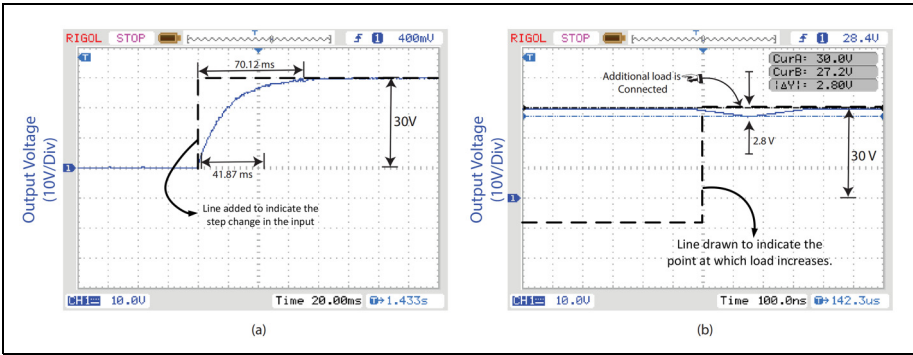


**Figure 5.** Experimental results for closed-loop system with PI controller. (a) Step response of the system. (b) Response of the system when additional load is connected.

**Table 3.** Comparison of different fixed-frequency SMC techniques.

Techniques	True parameter Independence	Analogue Digital	Cost	Convergence speed	Implementation Complexity	Sensed Parameters
Hysteresis band control SMC	Yes	Analogue	Medium	Real-time	Low	Voltage Current
Hysteresis mixed signal controller at constant switching frequency	Yes	Digital	High	Medium	High	Voltage Current
Zero averaged dynamics (ZAD)	Yes	Digital	High	Fast	High	Voltage Current
Second-order sliding mode controller	Yes	Digital	High	Medium	Medium	Voltage Current
Fixed-switching frequency integral sliding mode controller	No	Analogue	Low	Real-time	Medium	Voltage Current
Fixed-switching frequency using PWM	No	Analogue	Low	Real-Time	Medium	Voltage Current
Filter extracted equivalent control	Yes	Analogue	Low	Real-time	Low	Voltage Current
Double integral sliding mode control	Yes	Digital	Medium	Fast	High	Voltage Current
Dynamic integral sliding mode control	Yes	Digital	Medium	Fast	Low	Voltage Current

orbiting satellites, the dependability and performance are the highest priorities, with the cost and implementation complexity of the system being secondary considerations. Solar and electric vehicles require rapid convergence as well as low implementation costs, and in this scenario, analogue implementation is the most appropriate choice for these applications. When using PV arrays to power street lights, the controllers only have to charge the batteries during the day. As a result, they can be implemented utilizing procedures that are simple and minimally in cost.

To provide a guideline to the readers for general applications, the authors have gathered and summarized all the major characteristics of different fixed-frequency SMC techniques in Table 3, which should be consulted for selecting an appropriate method for a given particular application.

## Conclusion

The fundamental source of disturbance rejection in SMC-based systems is a discontinuous function. However, it causes frequency drifts, resulting in filter design problems related to EMC. This paper proposes a novel DISMC technique to fix the switching frequency in a power electronic converter while countering the effects of parametric variations and external perturbations. The control law is selected such that it incorporates an integral term that eliminates the reaching phase. The controller is tested under different load conditions and it is observed that the robustness is significantly improved. Experimental results are presented to validate the technique. Furthermore, a comprehensive comparison of different fixed-frequency SMC techniques along with their major characteristics have also been discussed in a tabular form. The comparison has been made on the basis of a few fundamental parameters allowing the readers to determine the feasibility of a technique to be used for a particular application.

## Acknowledgements

The authors thank all the members of the research lab at the University of Lahore.


## Declaration of conflicts of interests


The authors declared no potential conflicts of interest with respect to the research, authorship, and/or publication of this article.

## Funding

The authors received no financial support for the research, authorship and/or publication of this article.

## ORCID iDs

Mudassar Riaz  <https://orcid.org/0000-0003-4757-6595>

Abdul Rehman Yasin  <https://orcid.org/0000-0002-6754-6492>

## References

1. Al-Ghussain L, Samu R, Taylan O, et al. Sizing renewable energy systems with energy storage systems in microgrids for maximum cost-efficient utilization of renewable energy resources. *Sustain Cities Soc* 2020; 55: 102059.
2. Andreotti A, Petrillo A, Santini S, et al. A decentralized architecture based on cooperative dynamic agents for online voltage regulation in smart grids. *Energies* 2019; 12(7): 1386.
3. Ardjoun SAEM, Denai M and Abid M. A robust power control strategy to enhance lvr capability of grid-connected dfig-based wind energy systems. *Wind Energy* 2019; 22(6): 834–847.
4. Hasankhani A and Hakimi SM. Stochastic energy management of smart microgrid with intermittent renewable energy resources in electricity market. *Energy* 2021; 219: 119668.
5. Yasin AR, Yasin A, Riaz M, et al. Filter extracted sliding mode approach for dc microgrids. *Electronics* 2021; 10(16). doi: 10.3390/electronics10161882.
6. Alsmadi YM, Alqahtani A, Giral R, et al. Sliding mode control of photovoltaic based power generation systems for microgrid applications. *Int J Control* 2021; 94(6): 1704–1715.
7. Alsmadi YM, Utkin V, Haj-ahmed MA, et al. Sliding mode control of power converters: Dc/dc converters. *Int J Control* 2018; 91(11): 2472–2493.
8. Yang Q, Saeedifard M and Perez MA. Sliding mode control of the modular multilevel converter. *IEEE Trans Ind Electron* 2019; 66(2): 887–897.
9. Utkin V, Guldner J and Shi J. *Sliding mode control in electro-mechanical systems*. Boca Raton: CRC Press, 2009.
10. Yasin AR, Ashraf M, Bhatti AI, et al. Fixed frequency sliding mode control of renewable energy resources in dc micro grid. *Asian J Control* 2019; 21(4): 2074–2086.
11. Sabanovic A et al. Buck converter regulator operating in the sliding mode. In: Proceedings of PCI 1893.
12. Venkataramanan R. Sliding mode control of power converters. PhD Thesis, California Institute of Technology, 1986.
13. Carpita M and Marchesoni M. Experimental study of a power conditioning system using sliding mode control. *IEEE Trans Power Electron* 1996; 11(5): 731–742.
14. Hizarci H, Pekparlak U, Arifoglu U. Conducted emission suppression using an emi filter for grid-tied three-phase/level t-type solar inverter. *IEEE Access*, 2021; 9: 67417–67431.
15. Qi W, Li S, Tan SC, et al. Parabolic-modulated sliding-mode voltage control of a buck converter. *IEEE Trans Ind Electron* 2018; 65(1): 844–854.
16. Repecho V, Biel D, Ramos-Lara R, et al. Fixed-switching frequency interleaved sliding mode eight-phase synchronous buck converter. *IEEE Trans Power Electron* 2018; 33(1): 676–688.
17. Yao S, Gao G and Gao Z. On multi-axis motion synchronization: The cascade control structure and integrated smc–adrc design. *ISA Trans* 2021; 109: 259–268.
18. Yasin AR, Ashraf M and Bhatti AI. A novel filter extracted equivalent control based fixed frequency sliding mode approach for power electronic converters. *Energies* 2019; 12(5): 853.
19. Gao M, Wang D, Li Y, et al. Fixed frequency pulse-width modulation based integrated sliding mode controller for phase-shifted full-bridge converters. *IEEE Access* 2018; 6: 2181–2192.
20. Repecho V, Biel D and Arias A. Fixed switching period discrete-time sliding mode current control of a pmsm. *IEEE Trans Ind Electron* 2018; 65(3): 2039–2048.
21. Chincholkar SH, Jiang W and Chan CY. An improved pwm-based sliding-mode controller for a dc–dc cascade boost converter. *IEEE Trans Circuits Syst II: Express Briefs* 2018; 65(11): 1639–1643.
22. Li J, Liu Z and Su Q. Improved adaptive backstepping sliding mode control for a three-phase pwm ac–dc converter. *IET Control Theory Appl* 2019; 13(6): 854–860.

23. Repecho V, Biel D, Olm JM, et al. Switching frequency regulation in sliding mode control by a hysteresis band controller. *IEEE Trans Power Electron* 2017; 32(2): 1557–1569.
24. Ortiz-Castrillón JR, Mejía-Ruiz GE, Muñoz-Galeano N, et al. A sliding surface for controlling a semi-bridgeless boost converter with power factor correction and adaptive hysteresis band. *Appl Sci* 2021; 11(4): 1873.
25. Hoyos FE, Candelo-Becerra JE and Hoyos Velasco CI. Application of zero average dynamics and fixed point induction control techniques to control the speed of a dc motor with a buck converter. *Appl Sci* 2020; 10(5): 1807.
26. Muñoz JG, Angulo F and Angulo-Garcia D. Zero average surface controlled boost-flyback converter. *Energies* 2021; 14(1): 57.
27. Yasin A, Ashraf M and Bhatti A. Fixed frequency sliding mode control of power converters for improved dynamic response in dc micro-grids. *Energies* 2018; 11(10): 2799.
28. Li Z, Wang X, Kong M, et al. Bidirectional harmonic current control of brushless doubly fed motor drive system based on a fractional unidirectional converter under a weak grid. *IEEE Access* 2021; 9: 19926–19938.
29. Tan SC, Lai Y, Tse C, et al. A fixed-frequency pulsewidth modulation based quasi-sliding-mode controller for buck converters. *IEEE Trans Power Electron* 2005; 20(6): 1379–1392.
30. Abrishamifar A, Ahmad A and Mohamadian M. Fixed switching frequency sliding mode control for single-phase unipolar inverters. *IEEE Trans Power Electron* 2012; 27(5): 2507–2514.
31. Ye J, Malysz P and Emadi A. A fixed-switching-frequency integral sliding mode current controller for switched reluctance motor drives. *IEEE J Emerg Sel Top Power Electron* 2015; 3(2): 381–394.
32. Huerta SC, Alou P, Garcia O, et al. Hysteretic mixed-signal controller for high-frequency dc–dc converters operating at constant switching frequency. *IEEE Trans Power Electron* 2012; 27(6): 2690–2696.
33. Vidal-Idiarte E, Marcos-Pastor A, Garcia G, et al. Discrete-time sliding-mode-based digital pulse width modulation control of a boost converter. *IET Power Electron* 2015; 8(5): 708–714.
34. Yan WT, Ho CNM, Chung HSH, et al. Fixed-frequency boundary control of buck converter with second-order switching surface. *IEEE Trans Power Electron* 2009; 24(9): 2193–2201.

## Author biographies

**Mudassar Riaz** received his bachelor's and master's degrees in Electrical Engineering from the University of Lahore in 2018 and 2020, respectively. He is employed as a lab engineer/instructor at the Department of Electrical Engineering at the University of Lahore. His primary research interests are in the areas of control systems, robotics, power electronics, and their applications in renewable energy systems.

**Abdul Rehman Yasin** received his BSc and MSc degree in Electrical Engineering from the University of Engineering and Technology Lahore in 2006 and 2012, respectively. He received his PhD in Electrical Engineering from Capital University of Science & Technology in the year 2019. He is currently serving as an assistant professor in the Electrical Engineering Department at the University of Lahore. His fields of interest include control systems, sliding mode control, plasma science, and power electronics.

**Ali Arshad Uppal** received the MS degree in Computer Engineering from the University of Engineering and Technology Taxila, Pakistan, in 2012, and the PhD degree in Electrical

Engineering from the COMSATS Institute of Information Technology (CIIT), Islamabad, Pakistan, in 2016. He is also an assistant professor at COMSATS University Islamabad.

**Amina Yasin** got her MSc and MPhil in Applied Physics in 2004 and 2008, respectively from the University of Engineering and Technology Lahore, Pakistan. She is currently working as a lecturer in the Physics Department at King Faisal University, Al-Hasa, Saudi Arabia. Her area of interest is control systems and laser plasma.